Editors' Suggestion Featured in Physics

Observation of Large Unidirectional Rashba Magnetoresistance in Ge(111)

T. Guillet,[1] C. Zucchetti,[2] Q. Barbedienne,[3] A. Marty,[1] G. Isella,[2] L. Cagnon,[4] C. Vergnaud,[1] H. Jaffrès,[3] N. Reyren,[3] J.-M. George,[3] A. Fert,[3] and M. Jamet[1]

[1]Université Grenoble Alpes, CEA, CNRS, Grenoble INP, IRIG-SPINTEC, 38000 Grenoble, France
[2]LNESS-Dipartimento di Fisica, Politecnico di Milano, Piazza Leonardo da Vinci 32, 20133 Milano, Italy
[3]Unité Mixte de Physique, CNRS, Thales, Univ. Paris-Sud, Université Paris-Saclay, 91767, Palaiseau, France
[4]Université Grenoble Alpes, CNRS, Grenoble INP, Institut NEEL, 38000 Grenoble, France

(Received 4 June 2019; revised manuscript received 4 September 2019; published 13 January 2020)

Relating magnetotransport properties to specific spin textures at surfaces or interfaces is an intense field of research nowadays. Here, we investigate the variation of the electrical resistance of Ge(111) grown epitaxially on semi-insulating Si(111) under the application of an external magnetic field. We find a magnetoresistance term that is linear in current density j and magnetic field B, hence, odd in j and B, corresponding to a unidirectional magnetoresistance. At 15 K, for $I = 10\ \mu\text{A}$ (or $j = 0.33\ \text{A m}^{-1}$) and $B = 1$ T, it represents 0.5% of the zero field resistance, a much higher value compared to previous reports on unidirectional magnetoresistance (UMR). We ascribe the origin of this magnetoresistance to the interplay between the externally applied magnetic field and the pseudomagnetic field generated by the current applied in the spin-splitted subsurface states of Ge(111). This unidirectional magnetoresistance is independent of the current direction with respect to the Ge crystal axes. It progressively vanishes, either using a negative gate voltage due to carrier activation into the bulk (without spin-splitted bands), or by increasing the temperature due to the Rashba energy splitting of the subsurface states lower than $\sim 58 k_B$. We believe that UMR could be used as a powerful probe of the spin-orbit interaction in a wide range of materials.

DOI: 10.1103/PhysRevLett.124.027201

After decades of studies, spintronics has driven its most successful industrial revolutions in the read-out head of magnetic hard disk and in magnetic random access memory [1]. In both cases, a long-range magnetic order is the ultimate ingredient, since these applications rely on the giant magnetoresistance (GMR) effect [2,3]. Because of the seeking of magnetic ordering, the investigation of GMR has been wide and successful in ferromagnetic-based layers but still rare in semiconductors. Since a connection with magnetism in semiconductors would be desirable, lots of interest has been devoted to doping semiconductors with magnetic impurities [4,5]. The low solubility of magnetic ions [1] and Curie temperatures below 200 K [6] still limit the applicability of this technology. An alternative to long-range magnetic order in semiconductors comes from spin-orbit coupling (SOC), the main core of the so-called spin-orbitronics field in semiconducting films and in topological insulators [7,8].

Within this field, the investigation of magnetoresistance has recently moved over the standard ferromagnet-related effects [9–15], and a promising new type of magnetoresistance has been observed in the topological insulator Bi_2Se_3 [13], the two-dimensional electron gas at the $SrTiO_3(111)$ surface [15], and the polar semiconductor BiTeBr [16]. Since, in both cases, no magnetic order is present, the effect has been related to the characteristic spin-momentum locking [13–15]. The detected magnetoresistance exhibits two characteristic features: it is unidirectional (i.e., odd) and linear with the applied magnetic field and electrical current; therefore it has been classified among the unidirectional magnetoresistances (UMRs) [13–15]. Despite the same angular dependence, this SOC-related UMR has a different origin compared to another type of UMR recently investigated and involving a ferromagnetic layer [17–20].

Here, we report the observation of UMR in Ge(111). We ascribe its origin to the Rashba SOC, which generates spin-momentum locking inside the subsurface states of Ge(111). Their presence and spin texture have already been demonstrated exploiting angle and spin-resolved photoemission spectroscopy [21–24]. Experimentally, we find that the UMR in the Ge(111) subsurface states is drastically larger compared to previous reports [13,15]. We detect a maximum UMR value equivalent to 0.5% of the zero field resistance, when a magnetic field of 1 T and a current of 10 μA are applied at 15 K. The effect progressively vanishes when increasing the temperature or applying a negative gate voltage due to carrier activation in the bulk valence bands of Ge and to the low value of the Rashba spin-orbit coupling ($\sim 58 k_B$) [21].

We perform magnetotransport measurements on a 2 μm-thick Ge(111) using lithographically defined Hall bars (length $\ell = 120\ \mu$m, width $w = 30\ \mu$m, and aspect ratio $Z = \ell / w = 4$) as shown in Fig. 1(a) [25]. We apply a dc

 © 2020 American Physical Society

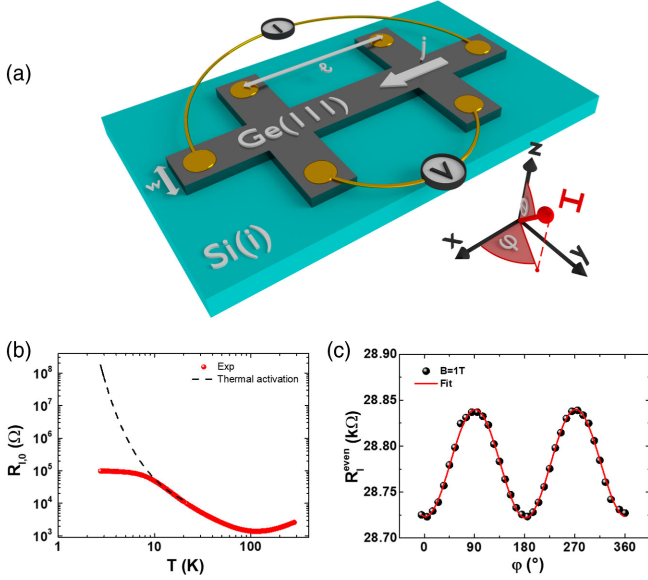

FIG. 1. Sketch of the double Hall cross used for magnetoresistance four-probe measurements. The external magnetic field is applied along (θ, φ) directions, θ and φ being the polar and azimuth angles. (b) Four-probe resistance versus temperature measured with an applied current of 10 μA. The red curve corresponds to experimental data exhibiting a resistance saturation; the dashed black line shows the expected semiconducting behavior considering a thermal activation of 2.6 meV. (c) Angular dependence in the (xy) plane of R_l^{even} at 15 K. The applied magnetic field is 1 Tesla and the current is 10 μA. The solid red line is a fit to the experimental data using a sine function.

charge current and measure the longitudinal and transverse resistances under the application of an external magnetic field $\mathbf{B}$. The direction of $\mathbf{B}$ is determined by its polar (θ) and azimuth (φ) angles as shown in Fig. 1(a). In dc measurements, the UMR term is odd with respect to the applied current and thus defined as $R_l^{\mathrm{odd}} = [R_l(I) - R_l(-I)]/2$. We also measure $R_t^{\mathrm{odd}} = [R_t(I) - R_t(-I)]/2$ and the longitudinal resistance that is even with respect to the applied current $R_l^{\mathrm{even}} = [R_l(I) + R_l(-I)]/2$. All the measurements are carried out as a function of the temperature from 15 to 295 K. The conductivity is p type in the whole temperature range; at 15 K the carrier density reaches $p \approx 6 \times 10^{15}$ cm^{-3}.

We report in Fig. 1(b) the four-probe temperature dependence of the zero magnetic field resistance $R_{l,0}$. The resistance plateau below 10 K differs from the purely thermally activated transport behavior one could expect from bulk Ge; therefore we interpret this observation as a fingerprint of a conduction channel in parallel with bulk conduction (black dashed line), as discussed in a similar situation of shorting by the surface states of topological insulators [27–30]. The angular dependence of R_l^{even} at 15 K in the (xy) plane is shown in Fig. 1(c) for $I = 10$ μA. This MR signal exhibits maxima (respectively minima) for $\mathbf{B}\|\hat{\mathbf{y}}$, $\varphi = 90°$ (respectively $\mathbf{B}\|\hat{\mathbf{x}}$, $\varphi = 0°$). Since the sign is not reversed when reversing the magnetic field direction, we call this term anisotropic magnetoresistance (AMR) by analogy with ferromagnets. At 15 K, we find an AMR of 0.4% under a magnetic field of 1 T. The same behaviors are obtained for angular dependencies within (zy) and (zx) planes. In Fig. 2, we report the angular dependence of R_l^{odd} and R_t^{odd} in the (xy), (xz), and (yz) planes for $B = 1$ T, $I = 10$ μA at 15 K. We observe a unidirectional behavior for both longitudinal and transverse resistances: the maximum (minimum) of R_l^{odd} is observed for $\mathbf{B}\|(\mp)\hat{\mathbf{y}}$, and the maximum (minimum) of R_t^{odd} is observed for $\mathbf{B}\|(\mp)\hat{\mathbf{x}}$. Thus, experimentally, $R_l^{\mathrm{odd}} = -R_{l,\max}^{\mathrm{odd}} \sin(\varphi)\sin(\theta)$ and $R_t^{\mathrm{odd}} = -R_{t,\max}^{\mathrm{odd}} \cos(\varphi)\sin(\theta)$. These functions are shown as solid lines in Fig. 2. R_t^{odd} angular dependence reveals the presence of the Nernst effect due to a current-induced vertical temperature gradient (along $\hat{\mathbf{z}}$) in the Ge(111) film. This effect generates spurious thermal UMR signal in the longitudinal resistance [31]. The Nernst effect contribution to R_l^{odd} can be written as $R_{l,\max}^{\mathrm{odd,Nernst}} = ZR_{t,\max}^{\mathrm{odd}}$, with Z being the aspect ratio of the channel ($Z = 4$ in our case) [18]. Hence, to remove the Nernst effect contribution from the longitudinal signal, we study $R_{\mathrm{UMR}} = R_{l,\max}^{\mathrm{odd}} - ZR_{t,\max}^{\mathrm{odd}}$ [25].

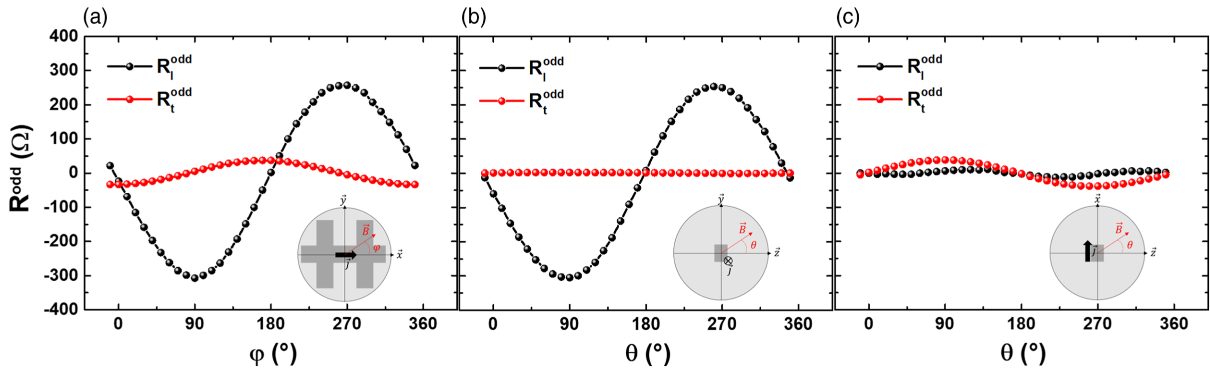

FIG. 2. Angular dependence of R_l^{odd} (black dots) and R_t^{odd} (red dots) in (a) the (xy) plane ($\theta = 90°$), (b) the (yz) plane ($\varphi = 90°$), and (c) the (xz) plane ($\varphi = 0°$), respectively. The temperature is 15 K, the applied current 10 μA, and the magnetic field 1 T. The solid black and red lines are fitting curves of R_l^{odd} and R_t^{odd}, respectively, using sine and cosine functions.

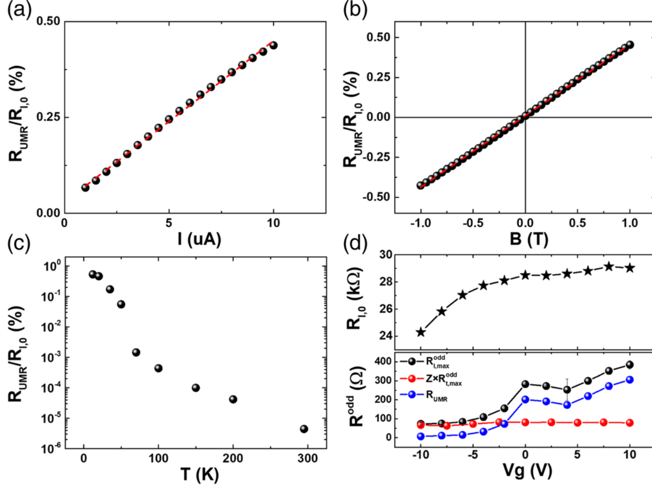

FIG. 3. R_{UMR} normalized to the zero magnetic field resistance $R_{l,0}$ taken at $\varphi = 270°$ (in %) as a function of (a) the applied current for $B = 1$ T and $T = 15$ K (b) the magnetic field for $I = 10$ μA and $T = 15$ K, and (c) the temperature for $B = 1$ T and $I = 10$ μA. Red dotted lines are linear fits. (d) Gate voltage dependence of $R_{l,0}$, $R^{\mathrm{odd}}_{l,\mathrm{max}}$, $ZR^{\mathrm{odd}}_{t,\mathrm{max}}$, and $R_{\mathrm{UMR}} = R^{\mathrm{odd}}_{l,\mathrm{max}} - ZR^{\mathrm{odd}}_{t,\mathrm{max}}$.

In Fig. 3 we investigate the dependencies of R_{UMR} on the applied current [Fig. 3(a)], magnetic field [Fig. 3(b)], temperature [Fig. 3(c)], and gate voltage [Fig. 3(d)]. The signal is normalized with respect to the zero field resistance $R_{l,0}$ at the corresponding current. In agreement with previous reports on UMR generated by spin-momentum locking [17,18] we observe a signal proportional to the current and the magnetic field. $R_{\mathrm{UMR}}/R_{l,0}$ is maximum and almost constant at low temperature ($T < 20$ K) and sharply decreases when the temperature becomes comparable to the Rashba spin-splitting energy (≈60 K). As shown in Fig. 3(d), the application of a top gate voltage modulates the channel resistance $R_{l,0}$. In Fig. 3(d), we also plot both the longitudinal and transverse odd resistance components as a function of the gate voltage. The transverse component we attribute to the Nernst effect stays constant with the gate voltage. This observation is consistent with the fact that this effect is due to vertical temperature gradient in the Ge(111) film and is almost unaffected by the top gate voltage. By contrast, $R^{\mathrm{odd}}_{l,\mathrm{max}}$ is much affected by the gate voltage: it increases from $V_g = -10$ V to $V_g = +10$ V by a factor ≈3. Therefore, after subtracting the longitudinal magnetoresistance component due to the Nernst effect ($ZR^{\mathrm{odd}}_{t,\mathrm{max}}$), we find that R_{UMR} cancels out at $V_g = -10$ V and increases by about 50% from $V_g = 0$ V to $V_g = +10$ V.

To make a comparison with previous results on different systems, we can define a figure of merit η. Since the UMR signal is proportional to the current and magnetic field, a natural definition is $\eta = R_{\mathrm{UMR}}/(R_{l,0}jB)$. At 15 K, in Ge (111), we obtain $\eta = 4.2 \times 10^{-7}$ cm^2/(A T) if we consider that the current completely flows within the spatial extension of the subsurface states (ten atomic layers from Ref. [23]). The value of η obtained in Ge(111) is orders of magnitude larger than the one of $SrTiO_3$ at 7 K [$\eta = 2 \times 10^{-9}$ cm^2/(A T) from Ref. [15]] and the one of Bi_2Se_3 at 60 K [$\eta = 2 \times 10^{-11}$ cm^2/(A T) from Ref. [13]]. Additionally, UMR was observed in the recently discovered topological insulator $\alpha - Sn$ where $\eta = 1.4 \times 10^{-9}$ cm^2/(A T) [32].

At variance with previously reported systems [13,15] the UMR is isotropic with respect to the direction of the current flow in the surface Brillouin zone (SBZ). In fact, in the data shown in Figs. 1–3, the current flows along the ΓM direction of the Ge(111) SBZ, but no difference, within the experimental error, is detected with the current flowing along other reciprocal lattice directions [25]. In Refs. [13,14], the magnetoresistance is affected by the direction of the current flow in the SBZ, indicating that, in such a case, the UMR originates from the hexagonal warping [13] or strong crystal field effects [15]. In the case of Ge, this contribution appears to be negligible. We thus propose an alternative mechanism, in which the UMR in Ge(111) results from a combination of the applied magnetic field and the pseudomagnetic field generated by the current applied in the spin-splitted subsurface states of Ge(111) shown in Fig. 4(a). Ge(111) subsurface states are located close to the top of the valence bands and can only contribute to transport in p-type Ge(111) [22]. This interpretation is supported by the fact that we do not observe this effect for n-type Ge(111) or for Ge (100) films [25,26]. It also explains the gate voltage dependence of R_{UMR} in Fig. 3(d). Applying negative gate voltage shifts the Fermi level down into the valence band, which leads to the activation of bulk conduction and $R_{\mathrm{UMR}} \approx 0$ Ω for $V_g = -10$ V. At variance, by ramping the gate voltage from -10 to $+10$ V, the Fermi level shifts into the subsurface states thus increasing R_{UMR}. Finally, this interpretation also explains the temperature dependence of the UMR. By increasing the temperature, bulk conduction in the valence band is activated and shorts the subsurface states. Moreover, the Rashba spin-orbit coupling of $\sim 58k_B$ in Ge subsurface states [22] becomes negligible with respect to k_BT suppressing spin-momentum locking.

For the Fermi level crossing the subsurface states as shown in Fig. 4(a), the Fermi contour is made of two concentric rings [C and D in Fig. 4(b)] with opposite spin helicities. To describe the magnetotransport inside the subsurface states, we consider the following model Hamiltonian:

$$\mathcal{H} = -\frac{\hbar^2 k^2}{2m^*} + \alpha(\mathbf{k} \times \sigma) \cdot \hat{\mathbf{z}} + g\mu_B \sigma \cdot \mathbf{B}, \tag{1}$$

with $\hbar$ being the reduced Planck constant, m^* the effective mass of holes in the subsurface states, α the Rashba spin-orbit interaction, σ the vector of Pauli matrices, g

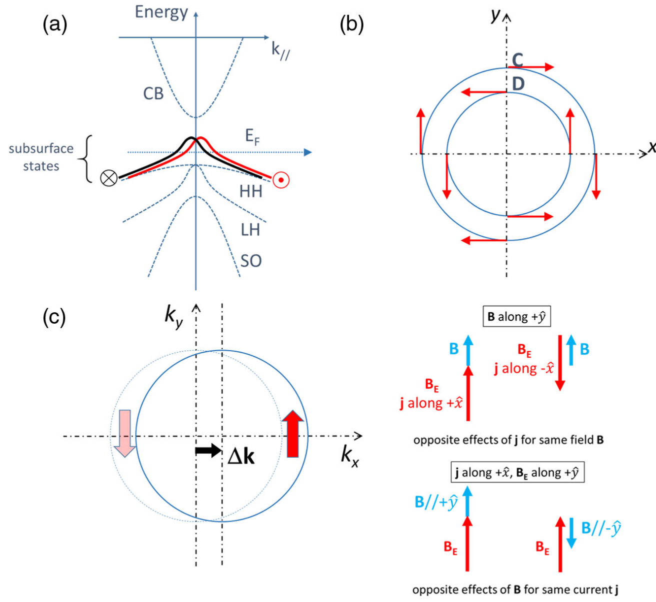

FIG. 4. (a) Schematics of the Ge(111) electronic band structure (in agreement with Ref. [22]) showing the bulk conduction and valence bands. The Fermi level is at a position corresponding to a p-doped film. Subsurface states are located just above the maximum of the bulk valence band and are crossed by the Fermi level. They are spin splitted by the Rashba and atomic spin-orbit interactions. (b) Fermi contours of the subsurface states. The outer (inner) contour is named C (D) with clockwise (counter-clockwise) spin helicity. (c) Illustration of the combined effects of the applied magnetic field $\mathbf{B}$ and the current dependent pseudo-magnetic field $\mathbf{B}_E$ on the resistivity of subsurface states for a single contour (D here). The contour is shifted by $+\Delta\mathbf{k}$ due to the application of a current density $\mathbf{j}$ along $+\hat{\mathbf{x}}$. The current direction and spin helicity set the pseudomagnetic field $\mathbf{B}_E$.

the Landé factor, and μ_B the Bohr magneton. When a two-dimensional charge current density $\mathbf{j}$ flows in the subsurface states, in the Boltzmann approach, the momentum acquires an extra component $\Delta\mathbf{k} = \beta\mathbf{j}$ with $\beta = 4\pi/(ev_F k_F)$, v_F and k_F being the Fermi velocity and wave vector we consider ($e = |e|$). A well-known consequence of such shifts of Rashba Fermi contours is the Rashba-Edelstein spin polarization [7,33] due to the unbalance between the opposite spin polarizations induced by the shifts in the same direction of the Rashba-splitted Fermi contours of opposite helicity. In parallel with the Rashba-Edelstein effect, the shift $\Delta\mathbf{k}$ introduces a current-induced out-of-equilibrium energy term that, from Eq. (1), is equal to $\alpha(\Delta\mathbf{k}\times\sigma)\cdot\hat{\mathbf{z}} = \alpha\beta(\mathbf{z}\times\mathbf{j})\cdot\sigma$ and acts on the spins as a pseudomagnetic field $\mathbf{B}_E = (\alpha\beta/g\mu_B)\hat{\mathbf{z}}\times\mathbf{j}$. As illustrated in Fig. 4(c), for a current along $\pm\hat{\mathbf{x}}$ with $\alpha > 0$, this field is directed along $\pm\hat{\mathbf{y}}$ and proportional to the current density. In the presence of an applied magnetic field $\mathbf{B}$, the spin of the subsurface states is submitted to $\mathbf{B} + \mathbf{B}_E$, $\mathbf{B}_E$ increasing or decreasing the effect of the y component of $\mathbf{B}$ for currents either along $+$ or $-\hat{\mathbf{x}}$. In the same way, still for $\alpha > 0$ for $\mathbf{j}$ along $+\hat{\mathbf{x}}$ and $\mathbf{B}_E$ along $\hat{\mathbf{y}}$, there is addition or subtraction of the effects of $\mathbf{B}$ and $\mathbf{B}_E$ for opposite orientations of $\mathbf{B}$ along $\hat{\mathbf{y}}$. The physics of the UMR thus comes from the pseudofield $\mathbf{B}_E$ induced by the out-of-equilibrium situation of a current flow and acting on the spins. We can go a little further by assuming that the AMR term shown in Fig. 1(c) (the only MR in the limit $j \to 0$) is also due to the effect of $\mathbf{B}$ on the spins. We thus follow Taskin *et al.* [34] who explain the AMR in systems with spin-momentum locking by the freezing of backscattering (partial freezing for Rashba 2DEG) at zero field (low resistance) and the anisotropic reintroduction of some backscattering and anisotropic reintroduction of resistance by the partial realignment of the locked spin by the magnetic field. We thus assume that the AMR comes only from the interaction of $\mathbf{B}$ with the spins and neglects other contributions such as the effect of the Lorentz force on the trajectories. Then, in the situation of finite j, we add $\mathbf{B}_E$ to $\mathbf{B}$ in the B^2 term of the AMR to derive the expression of UMR. The AMR term can be written as

$$(\Delta R/R)_{\mathrm{AMR}} = -AB^2\cos^2(\varphi) = AB_y^2 - AB^2, \quad (2)$$

where $A \approx 0.004$. Adding $B_{Ey} = \alpha\beta j/g\mu_B$ to B_y, and keeping only the terms of first order in j gives

$$\Delta R/R = -AB^2\cos^2(\varphi) + 2A(\alpha\beta/g\mu_B)jB\sin(\varphi), \quad (3)$$

where the second term, proportional to jB, is the UMR. Our experimental results with an UMR proportional to $jB\sin(\varphi)$, see Fig. 2, correspond to a negative value of the Rashba coefficient α, that is, to the clockwise chirality of the spin orientation in the outer Fermi contour. This chirality is in agreement with the chirality derived from spin-resolved ARPES measurements for the subsurface states inside Ge at Ge/Bi interfaces, as shown in Fig. 3(a) of [21]. Quantitatively, we can estimate the UMR amplitude by taking reasonable values for the parameters. By setting $B = 1$ T, $j = 0.33$ A m^{-1} in the subsurface states, $\alpha = -0.2$ eV Å (in [21], this value corresponds to Bi covered subsurface states; in our case it is probably an upper bound), $k_F = 0.025$ Å^{-1} (Rashba splitting $|\alpha k_F| = 5$ meV $\sim 58k_B$), $m^* = 0.4m_e$ [35], m_e being the electron mass, $v_F = \hbar k_F/m^*$ and $g = 2$, we find a UMR amplitude of ≈0.2%. This value is in good agreement with our low-temperature experimental data. We indeed find a maximum value of 0.5% at 15 K. Therefore, by using simple arguments, we capture the physics of UMR in the Ge Rashba-splitted subsurface states.

In conclusion, we performed magnetoresistance measurements on Ge(111) and detected a UMR that scales linearly with both the current and the applied magnetic field. We ascribe the UMR to the spin-momentum locking generated by the Rashba effect in the subsurface states of Ge(111) and interpret our results in a simple model relating the UMR to the Rashba coefficient and the characteristic

parameters of the subsurface states. Such unidirectional effects can be expected in any Rashba 2DEG and can be used to obtain information about the electronic structure details. The amplitude of the detected UMR signal is much larger than the ones previously reported. We also showed that this UMR is tunable by turning on and off the Rashba coupling in the conduction channel by applying a gate voltage. Ultimately, these findings lead towards the development of a semiconductor-based spin transistor where the spin information can be manipulated by a gate-tunable Rashba field.

The authors acknowledge the financial support from the ANR Grant No. ANR-16-CE24-0017 TOPRISE. One of us (A. F.) acknowledges fruitful discussions with A. Dyrdal and J. Barnas (Poznan University), as well as with S. Zhang (University of Arizona).

[1] J. Åkerman, Science **308**, 508 (2005).
[2] M. N. Baibich, J. M. Broto, A. Fert, F. Nguyen Van Dau, F. Petroff, P. Etienne, G. Creuzet, A. Friederich, and J. Chazelas, Phys. Rev. Lett. **61**, 2472 (1988).
[3] G. Binasch, P. Grünberg, F. Saurenbach, and W. Zinn, Phys. Rev. B **39**, 4828(R) (1989).
[4] H. Ohno, Science **281**, 951 (1998).
[5] T. Dietl, H. Ohno, F. Matsukura, J. Cibert, and D. Ferrand, Science **287**, 1019 (2000).
[6] L. Chen, X. Yang, F. Yang, J. Zhao, J. Misuraca, P. Xiong, and S. von Molnŕ, Nano Lett. **11**, 2584 (2011).
[7] C. Chappert, A. Fert, and F. N. Van Dau, Nat. Mater. **6**, 813 (2007).
[8] A. Manchon, H. C. Koo, J. Nitta, S. M. Frolov, and R. A. Duine, Nat. Mater. **14**, 871 (2015).
[9] N. Locatelli, V. Cros, and J. Grollier, Nat. Mater. **13**, 11 (2014).
[10] J. Kim, P. Sheng, S. Takahashi, S. Mitani, and M. Hayashi, Phys. Rev. Lett. **116**, 097201 (2016).
[11] I. Latella and P. Ben-Abdallah, Phys. Rev. Lett. **118**, 173902 (2017).
[12] Z. Qiu, D. Hou, J. Barker, K. Yamamoto, O. Gomonay, and E. Saitoh, Nat. Mater. **17**, 577 (2018).
[13] P. He, S. S.-L. Zhang, D. Zhu, Y. Liu, Y. Wang, J. Yu, G. Vignale, and H. Yang, Nat. Phys. **14**, 495 (2018).
[14] S. S.-L. Zhang and G. Vignale, arXiv:1808.06339v1.
[15] P. He, S. M. Walker, S. S.-L. Zhang, F. Y. Bruno, M. S. Bahramy, J. M. Lee, R. Ramaswamy, K. Cai, O. Heinonen, G. Vignale, F. Baumberger, and H. Yang, Phys. Rev. Lett. **120**, 266802 (2018).
[16] T. Ideue, K. Hamamoto, S. Koshikawa, M. Ezawa, S. Shimizu, Y. Kaneko, Y. Tokura, N. Nagaosa, and Y. Iwasa, Nat. Phys. **13**, 578 (2017).
[17] K. Olejnik, V. Novák, J. Wunderlich, and T. Jungwirth, Phys. Rev. B **91**, 180402(R) (2015).
[18] C. O. Avci, K. Garello, A. Ghosh, M. Gabureac, S. F. Alvarado, and P. Gambardella, Nat. Phys. **11**, 570 (2015).
[19] K. Yasuda, A. Tsukazaki, R. Yoshimi, K. S. Takahashi, M. Kawasaki, and Y. Tokura, Phys. Rev. Lett. **117**, 127202 (2016).
[20] Y. Lv, J. Kally, D. Zhang, J. S. Lee, M. Jamali, N. Samarth, and J.-P. Wang, Nat. Commun. **9**, 111 (2018).
[21] Y. Ohtsubo, S. Hatta, K. Yaji, H. Okuyama, K. Miyamoto, T. Okuda, A. Kimura, H. Namatame, M. Taniguchi, and T. Aruga, Phys. Rev. B **82**, 201307(R) (2010).
[22] Y. Ohtsubo, K. Yaji, S. Hatta, H. Okuyama, and T. Aruga, Phys. Rev. B **88**, 245310 (2013).
[23] T. Aruga, J. Electron Spectrosc. Relat. Phenom. **201**, 74 (2015).
[24] K. Yaji, Y. Ohtsubo, S. Hatta, H. Okuyama, R. Yukawa, I. Matsuda, P. Le Fèvre, F. Bertran, A. Taleb-Ibrahimi, A. Kakizaki, and T. Aruga, J. Electron Spectrosc. Relat. Phenom. **201**, 92 (2015).
[25] See Supplemental Material at http://link.aps.org/supplemental/10.1103/PhysRevLett.124.027201, for control experiments, which includes Ref. [26].
[26] C. Jeon, C. C. Hwang, T.-H. Kang, K.-J. Kim, B. Kim, Y. Chung, and C. Y. Park, Phys. Rev. B **74**, 125407 (2006).
[27] T. Liu, Y. Li, L. Gu, J. Ding, H. Chang, P. A. Praveen Janantha, B. Kalinikos, V. Novosad, A. Hoffmann, R. Wu, C. L. Chien, and M. Wu, Phys. Rev. Lett. **120**, 207206 (2018).
[28] T. Guillet, A. Marty, C. Beigné, C. Vergnaud, M.-T. Dau, P. Noël, J. Frigerio, G. Isella, and M. Jamet, AIP Adv. **8**, 115125 (2018).
[29] P. Noël, C. Thomas, Y. Fu, L. Vila, B. Haas, P.-H. Jouneau, S. Gambarelli, T. Meunier, P. Ballet, and J. P. Attane, Phys. Rev. Lett. **120**, 167201 (2018).
[30] S. Cai, J. Guo, V. A. Sidorov, Y. Zhou, H. Wang, G. Lin, X. Li, Y. Li, K. Yang, A. Li, Q. Wu, J. Hu, S. K. Kushwaha, R. J. Cava, and L. Sun, npj Quantum Mater. **3**, 62 (2018).
[31] N. Roschewsky, E. S. Walker, P. Gowtham, S. Muschinske, F. Hellman, S. R. Bank, and S. Salahuddin, Phys. Rev. B **99**, 195103 (2019).
[32] Q. Barbedienne *et al.* (to be published).
[33] V. M. Edelstein, Solid State Commun. **73**, 233 (1990).
[34] A. A. Taskin, H. F. Legg, F. Yang, S. Sasaki, Y. Kanai, K. Matsumoto, A. Rosch, and Y. Ando, Nat. Commun. **8**, 1340 (2017).
[35] See http://www.ioffe.ru.